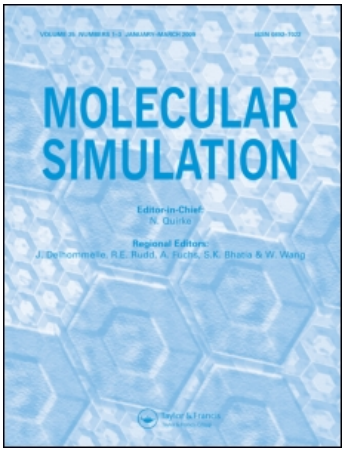

Molecular Simulation
Publication details, including instructions for authors and subscription information:
http://www.informaworld.com/smpp/title~content=t713644482

Heat transfer simulation using energy conservative dissipative particle dynamics

Eiyad Abu-Nada[ab]
[a] Department of Mechanical Engineering, Hashemite University, Zarqa, Jordan [b] Leibniz Universität Hannover, Institut für Technische Verbrennung, Hannover, Germany

Online publication date: 16 April 2010

To cite this Article Abu-Nada, Eiyad(2010) 'Heat transfer simulation using energy conservative dissipative particle dynamics', Molecular Simulation, 36: 5, 382 — 390
To link to this Article: DOI: 10.1080/08927020903515337
URL: http://dx.doi.org/10.1080/08927020903515337

Molecular Simulation
Vol. 36, No. 5, April 2010, 382–390

Taylor & Francis
Taylor & Francis Group

Heat transfer simulation using energy conservative dissipative particle dynamics

Eiyad Abu-Nada*

Department of Mechanical Engineering, Hashemite University, Zarqa 13115, Jordan; Leibniz Universität Hannover, Institut für Technische Verbrennung, Welfengarten 1a, 30167 Hannover, Germany

(*Received 5 October 2009; final version received 29 November 2009*)

Dissipative particle dynamics with energy conservation (eDPD) was used to investigate conduction heat transfer in two dimensions under steady-state condition. Various types of boundary condition were implemented to the conduction domain. Besides, 2D conduction with internal heat generation was studied and the heat generation term was used to measure the thermal conductivity and diffusivity of the eDPD system. The boundary conditions used include both the Neumann and Dirichlet boundary conditions. The Neumann boundary condition was applied via adiabatic surfaces and surfaces exposed to convection heat transfer. The DPD simulations were compared to analytical solutions and finite-difference techniques. It was found that DPD appropriately predicts the temperature distribution in the conduction regime. Details of boundary condition implementation and thermal diffusivity measurement are also described in this paper.

Keywords: dissipative particle dynamics; eDPD; boundary conductions; heat generation; thermal diffusivity

1. Introduction

Dissipative particle dynamics (DPD) is a particle-based mesoscopic simulation method introduced by Hoogerbrugge and Koelman [1], which captures hydrodynamics of fluid flow. DPD can predict complex hydrodynamics with a much higher computational efficiency compared to MD as each DPD particle represents a group or packet of actual molecules [2–4]. Since its introduction, DPD has been applied to simulate the behaviour of various complex fluid applications [5–14]. However, the DPD method was limited to isothermal systems and modelling of thermal systems was not possible because the total energy of the DPD system was not conserved. Español [15] and Avalos and Mackie [16] solved this energy conservation drawback and extended the isothermal DPD equations to model heat transport by introducing additional property to the DPD system, which is the internal energy. This energy conservation DPD system is known in the literature as eDPD. Therefore, in the eDPD system, each DPD particle is prescribed by the internal energy in addition to other quantities found in the convectional DPD system (mass, position and velocity). As a result, the heat transfer can be modelled by the change of eDPD particles' internal energy. The eDPD approach was applied to model various heat transfer problems [17–22]. Ripoll et al. [17] and Ripoll and Español [18] studied heat transfer in a 1D conduction domain and their results were compared with analytical solution of the heat conduction equation, and a good match between the two methods was reported. Also, they studied transport quantities such as thermal diffusivity for the 1D system. Mackie et al. [22] applied the eDPD approach to heat flow. More recently, the eDPD method was applied to model heat transfer in nanocomposites by Qiao and He [19] and heat transfer in nanoparticle suspensions by He and Qiao [20]. Also, Chaudhri and Lukes [21] extended the eDPD formulation to multi-components and applied it to the heat equation and 2D heat conduction. In their 2D model, they used Dirichlet boundary condition to model conduction in a 2D slab and compared their results with analytical solutions. As compiled from the literature search, the studies conducted using eDPD to model heat transport are still limited, and it is very important to apply eDPD to more thermal problems to promote the eDPD method as a powerful tool that could mimic various heat transfer applications. Besides, the implementation of boundary conditions is a very vital step in DPD simulations since the overall accuracy of the DPD solution depends on the boundary condition implementation. Therefore, it is of importance to present a study that focuses on the boundary condition implementation in eDPD simulations. In essence, the ultimate goal of the eDPD model is to model convection heat transfer applications at the mesoscale and such modelling requires implementation and testing various types of boundary condition on the eDPD system to model convection heat transfer accurately. Therefore, the objective of the current work is to investigate conduction heat transfer in two dimensions using various types of boundary condition and to measure thermal conductivity and diffusivity of the eDPD system. The 2D domain will be exposed to various types of boundary condition such as adiabatic and convection boundary

*Email: eiyad@hu.edu.jo

ISSN 0892-7022 print/ISSN 1029-0435 online

DOI: 10.1080/08927020903515337
http://www.informaworld.com

conditions. The current eDPD simulations will be compared with analytical and finite-difference solutions to test the validity of the simulations.

2. eDPD governing equations

Basically, similar to the convectional DPD approach, the eDPD method is a particle method based on pairwise interactions between a particle and neighbouring particles within a certain cut-off radius. The eDPD particles are still considered as a coarse-grained particle where each eDPD particle resembles a group of actual fluid molecules. The time evolution of eDPD particles is governed by conservation of momentum and energy and is described by the following set of equations [15,19,20]:

$$\frac{\mathrm{d}\vec{r}_i}{\mathrm{d}t} = \vec{v}_i, \tag{1}$$

$$m_i \frac{\mathrm{d}\vec{v}_i}{\mathrm{d}t} = \left(\vec{f}_{ij}^{\,\mathrm{C}} + \vec{f}_{ij}^{\,\mathrm{D}} + \vec{f}_{ij}^{\,\mathrm{R}}\right), \tag{2}$$

$$C_v \frac{\mathrm{d}T_i}{\mathrm{d}t} = \left(q_{ij}^{\mathrm{visc}} + q_{ij}^{\mathrm{cond}} + q_{ij}^{\mathrm{R}}\right). \tag{3}$$

The conservative force $\vec{f}_{ij}^{\,\mathrm{C}}$, dissipative force $\vec{f}_{ij}^{\,\mathrm{D}}$ and random force $\vec{f}_{ij}^{\,\mathrm{R}}$ are expressed as [2,12,14]:

$$\vec{f}_{ij}^{\,\mathrm{C}} = \sum_{j\neq i} a_{ij} w(r_{ij}) \vec{e}_{ij}, \tag{4}$$

$$\vec{f}_{ij}^{\,\mathrm{D}} = \sum_{j\neq i} -\gamma_{ij} w^2(r_{ij}) (\vec{e}_{ij}\cdot\vec{v}_{ij}) \vec{e}_{ij}, \tag{5}$$

$$\vec{f}_{ij}^{\,\mathrm{R}} = \sum_{j\neq i} \sigma_{ij} w(r_{ij}) \zeta_{ij} \Delta t^{-1/2} \vec{e}_{ij}. \tag{6}$$

Also, the heat flux vectors q_{ij}^{visc}, q_{ij}^{cond}, q_{ij}^{R} account for viscous, collision and random heat fluxes, respectively, and are given by [15,19,20]:

$$q_{ij}^{\mathrm{cond}} = \sum_{j\neq i} \kappa_{ij} w^2(r_{ij}) \left(\frac{1}{T_i} - \frac{1}{T_j}\right), \tag{7}$$

$$q_{ij}^{\mathrm{visc}} = \sum_{j\neq i} \frac{1}{2C_v} \left(w^2(r_{ij}) \left[\gamma_{ij} (\vec{e}_{ij}\cdot\vec{v}_{ij})^2 - \frac{\sigma_{ij}^2}{m}\right] - \sigma_{ij} w(r_{ij}) (\vec{e}_{ij}\cdot\vec{v}_{ij}) \zeta_{ij} \right), \tag{8}$$

$$q_{ij}^{\mathrm{R}} = \sum_{j\neq i} \alpha_{ij} w(r_{ij}) \Delta t^{-1/2} \zeta_{ij}^{e}, \tag{9}$$

where $r_{ij} = r_i - r_j$ and $v_{ij} = v_i - v_j$; e_{ij} is the unit vector pointing in the direction from j to i. The parameter a_{ij} is a repulsion parameter between the eDPD particles. Also, γ_{ij} and σ_{ij} in Equations (5) and (6) are the strength of dissipative and random forces, respectively. Also, κ_{ij} and α_{ij} in Equations (7) and (9) determine the strength of the collisional and random heat fluxes [15,19,20]. The weight function w decreases monotonically with the particle–particle separation distance. It becomes zero beyond the cut-off length and, in the current work, a linear weighting function is used which is given as

$$w(r_{ij}) = \begin{cases} (1 - (r_{ij}/r_{\mathrm{c}})) & (r_{ij} < r_{\mathrm{c}}), \\ 0 & (r_{ij} \geq r_{\mathrm{c}}). \end{cases} \tag{10}$$

The random number ζ_{ij} that appears in Equation (6) has a zero mean and a unit variance and has the property $\zeta_{ij} = \zeta_{ji}$ to ensure the conservation of the total momentum of the DPD system [1,2,4,5,7,12]. However, ζ_{ij}^{e} is a non-symmetrical random number with a zero mean and a unit variance [15]. The relation between the parameters γ_{ij} and σ_{ij} is governed by the fluctuation–dissipation theorem [15],

$$\gamma_{ij} = \frac{\sigma_{ij}^2 (T_i + T_j)}{4k_{\mathrm{B}} T_i T_j}, \tag{11}$$

$$\alpha_{ij} = \sqrt{2k_{\mathrm{B}}\kappa_{ij}}, \tag{12}$$

where k_{B} is the Boltzmann constant. The parameter κ_{ij} is given as

$$\kappa_{ij} = \frac{C_v^2 k_o (T_i + T_j)^2}{4k_{\mathrm{B}}}, \tag{13}$$

where k_o is interpreted as heat friction that controls thermal conductivity [17–20]. Also, C_v is the heat capacity at constant volume for an eDPD bead. In general, the heat capacity of the eDPD particles is normalised by the Boltzmann constant to give a non-dimensional number $\bar{C}_v = C_v/k_{\mathrm{B}}$. The mass of the eDPD particles and the cut-off radius r_{c} are set to unity in the present simulations.

3. Validation of the eDPD code

The present eDPD code is validated by simulating two fundamental heat transfer problems and comparing the current eDPD results with analytical solutions. The first problem is transient heat conduction in a 1D slab governed by the heat equation. This problem was also used for validation by previous researchers [17–21]. The eDPD particles are uniformly distributed in a 2D lattice, where the x and y spacings are taken as 0.5. To drive the heat transfer, a temperature gradient is imposed between two given reservoirs in this case, the top and bottom walls of the slab. The top and bottom walls are represented by two layers of the eDPD particles having the same spacing as the interior domain. The temperatures of the bottom and top walls are set, respectively, to 2.0 and 1.0. The periodic boundary condition is used in the x direction. Initially, all

of the eDPD particles are assigned an initial temperature of 1.5. The dimensionless heat capacity of the eDPD particles ($\bar{C}_v$) is set to 1×10^5 [19]. The computational domain is divided into 20×20 number of unit cells in the x and y directions, respectively. The number density is fixed at 4.0. The time step is kept very fine to capture the evolution of temperature distribution in the domain. The analytical solution is given by [23]:

$$T(y,t) = 1 + \frac{y}{L} + \frac{2}{\pi}\sum_{n=1}^{\infty}\frac{2\cos(n\pi)-1}{n} \times \sin\left(\frac{n\pi y}{L}\right)\exp\left(-\frac{Dn^2\pi^2 t}{L^2}\right) - \frac{3}{\pi}\sum_{n=1}^{\infty}\frac{\cos(n\pi)-1}{n}\sin\left(\frac{n\pi y}{L}\right)\exp\left(-\frac{Dn^2\pi^2 t}{L^2}\right), \quad (14)$$

where L is the domain height (distance between the top and bottom walls), which is 20 for this case, and D is the diffusivity. Figure 1 presents a comparison between the DPD and analytical solution where a good comparison is observed.

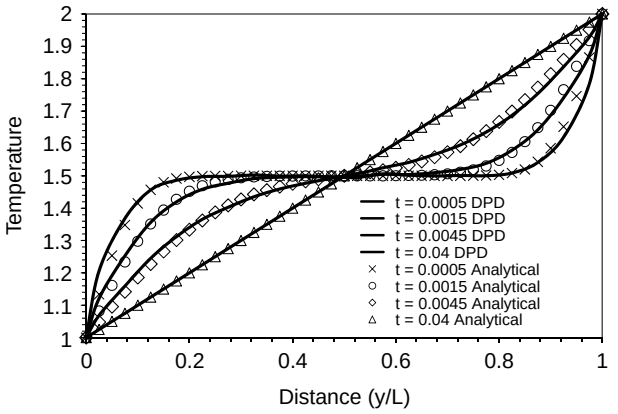

Figure 1. Temperature evolution in a 1D slab: comparison between the current eDPD code and analytical solutions.

The second problem of validation is a simulation of steady-state 2D conduction in a slab. This problem has a fixed-form analytical solution and has been used by Chaudhri and Lukes [21] to validate their multicomponent eDPD model. A sketch of the problem geometry and the corresponding boundary condition of this problem are

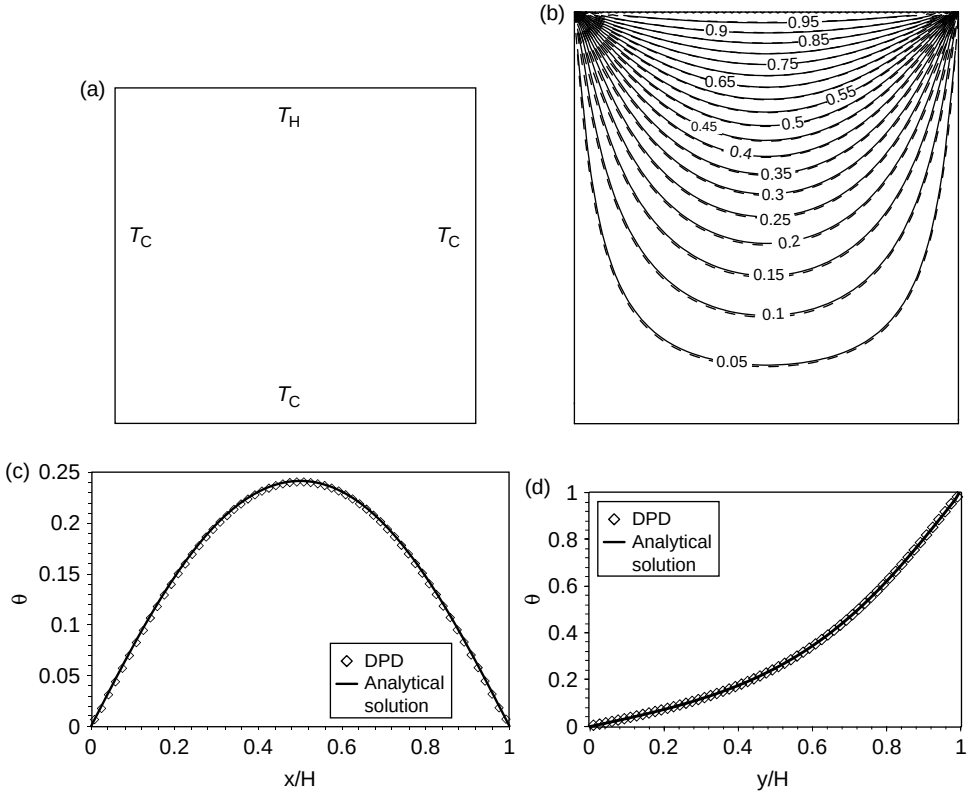

Figure 2. (a) Sketch of the problem geometry for the validation of the 2D eDPD code. (b) Temperature isotherms (solid line, DPD; dashed line, analytical solution). (c) Temperature profiles at the mid-slab height (i.e. $y = 20$). (d) Temperature profiles at the mid-slab width (i.e. $x = 20$).

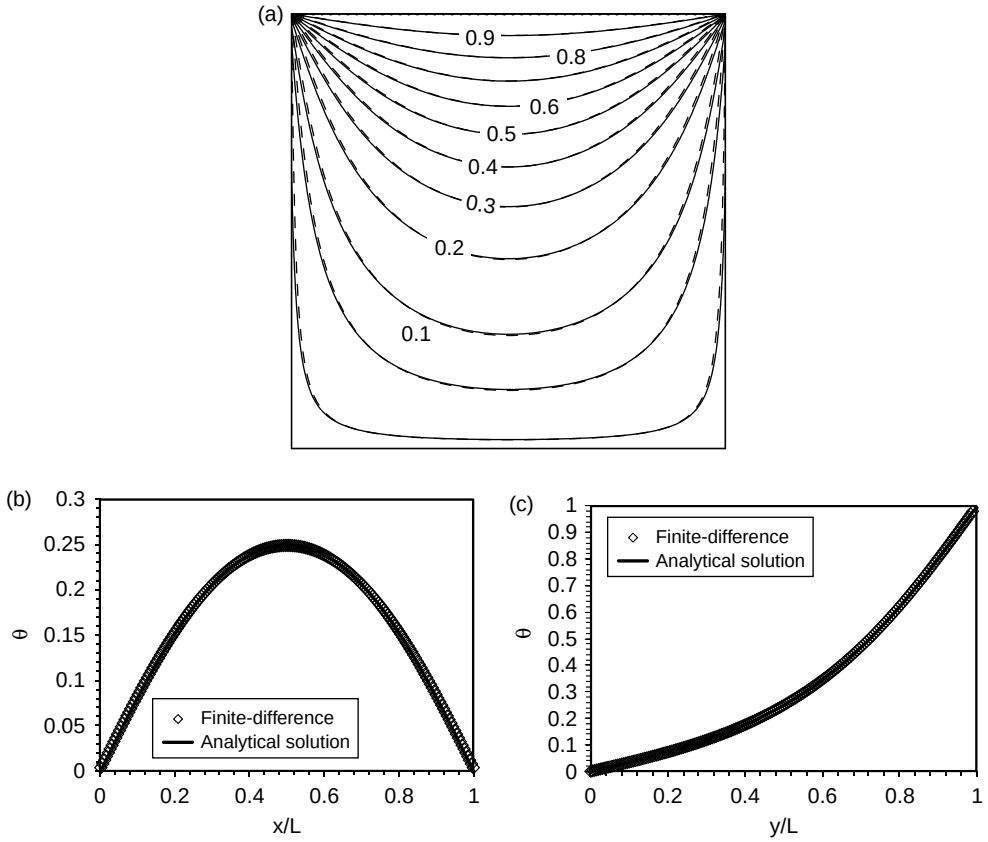

Figure 3. Validation of the finite-difference solution against analytical solution. (a) Temperature isotherms (solid line, finite-difference; dashed line, analytical solution). (b) Temperature profiles at the mid-slab height. (c) Temperature profiles at the mid-slab width.

shown in Figure 2(a). The steady-state 2D heat conduction equation is given as [24]:

$$\frac{\partial^2 T}{\partial x^2} + \frac{\partial^2 T}{\partial y^2} = 0. \tag{15}$$

The analytical solution of Equation (15) is given as [24]:

$$T(x,y) = \frac{2}{\pi}\sum_{n=1}^{\infty} \frac{(-1)^{n+1}+1}{n} \sin\left(\frac{n\pi x}{H}\right) \frac{\sinh(n\pi y/H)}{\sinh(n\pi W/H)}, \tag{16}$$

where H and W are the height and width of the slab, respectively (here $H = W$). The number density is set to 4.0 and the temperatures of the hot and the cold walls are set to 25 and 1.0, respectively. To mimic the large gradients experienced at the wall surfaces, the computation domain is divided into a large number of unit cells (40×40) in the x and y directions. However, the use of a small number of unit cells (e.g. 10×10) still captures the correct physics of the problem. The following non-dimensional temperature is introduced to compare the DPD with the analytical solution:

$$\theta = \frac{T - T_C}{T_H - T_C}, \tag{17}$$

where T is the dimensional temperature and T_C and T_H are the cold and hot temperatures of the reservoirs, respectively. The particles are uniformly distributed in the 2D lattice where the x and y spacings are taken as 0.5. All walls are represented by two layers of the eDPD particles using the same spacing as the interior domain. As reflected from Figure 2(b)–(d), the comparison between the eDPD and analytical solutions is excellent.

In the following sections, the eDPD results will be compared with finite-difference solutions. So, it is worth presenting a validation of the finite-difference solution scheme against the analytical solution given in Equation (16). The finite-difference solution depends on the discretisation of Equation (15) absorbing the boundary conditions portrayed in Figure 2(a). Figure 3 shows a comparison between the finite-difference and analytical solution, where both methods give almost exactly similar results which give a confidence to use the finite-difference to validate the eDPD simulation presented in the following section.

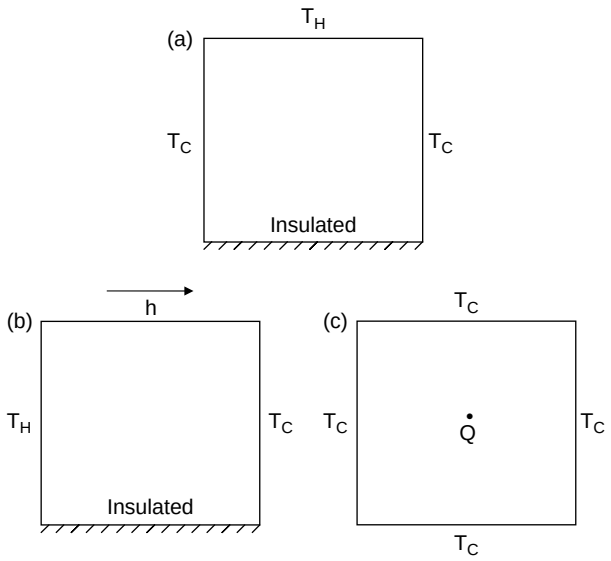

Figure 4. Sketch of problem geometries: (a) case I, (b) case II and (c) case III.

4. Results and discussion

In this section, three different heat conduction problems in two dimensions are studied using the eDPD approach and compared with finite-difference solutions. The first problem (case I) presents heat conduction in a slab where one of the walls is subjected to adiabatic boundary condition. The second problem (case II) describes implementation of convection heat transfer boundary condition to conduction problems. Finally, the last problem (case III) describes heat generation in a slab and the calculation procedure of the thermal conductivity and thermal diffusivity of the eDPD system. Figure 4 shows a schematic diagram of the three different cases under study.

4.1 Case I

The geometry and the corresponding boundary condition for this problem are shown in Figure 4(a). The left, right and top walls are treated similarly to the procedure outlined in Section 3. However, the bottom wall has a different treatment since an adiabatic boundary condition is used. Since an adiabatic boundary condition means a symmetry condition, this means that the distribution of the wall boundary particles located in the two extra layers must be a mirror image of the corresponding particles in the interior eDPD particles. If uniformly distributed particle is used, this is automatically guaranteed since the same particle spacing is used for the wall eDPD particles as interior particle spacing. However, care must be taken when interior particles are randomly distributed since the location of particles in the first layer adjacent to the wall cells has to be saved and a mirror location of these particles has to be created to generate the corresponding wall eDPD particles. This becomes of importance for convection problems where all interior eDPD particles are moving and therefore the location of the particles in the first layer adjacent to the adiabatic wall keeps changing with time. Therefore, the location of the wall particles is not any longer kept fixed and is updated for each time step accordingly. In the present work, the algorithm used is programmed to check the location of the eDPD particles adjacent to the adiabatic wall, and a mirror image of these particles is created in the wall boundary to allocate the wall particles. Both approaches of random and uniform distribution of particles in the interior domain are tested and shown to give similar results, but due to the limited space in this paper, such a comparison is not presented.

Mathematically, the adiabatic boundary condition is given as $\mathrm{d}T/\mathrm{d}y = 0$. A second-order accurate forward difference formula for the first derivative at the bottom wall is expressed as

$$\frac{\mathrm{d}T}{\mathrm{d}y} = \frac{-3T_{1,j} + 4T_{2,j} - T_{3,j}}{2\Delta y}, \tag{18}$$

where 1, 2 and 3 correspond to the boundary, the first cell and the second cell of the interior domain and Δy is the unit cell width which is equal to unity in the present work. Therefore, solving for the temperature of the boundary, the following formula is obtained:

$$T_{1,j} = \frac{4T_{2,j} - T_{3,j}}{3}. \tag{19}$$

Therefore, the temperature of the wall eDPD particles is expressed as a function of the interior eDPD particles, namely in the first and the second cells adjacent to the wall boundary. Therefore, the temperature of the wall particles is solved for each time step similar to the interior domain particles.

To carry out the eDPD simulation, the computation domain is divided into a number of unit cells (40×40). As the forces are effective within the cut-off radius, particles far from r_c are excluded in the computation. A cell division and link-list approach is implemented to enhance the computational efficiency [25]. The time step is kept small as 0.00002 and the total time steps used to reach the steady state are 100,000 steps. The reason for using a small time step is that a large heat capacity ($\bar{C}_v = 100,000$) is used. The value of k_o (heat friction) is kept constant at 0.1. Also, the strength of the random forces parameter (σ_{ij}) is set to 3.0. The statistical averaging of the eDPD parameters (temperature in this case) is carried out by dividing each unit cell into two bins and data is averaged in the last 25,000 time steps. The temperature is non-dimensionalised according to Equation (17). Figures 5 and 6(a), (b) show comparison for the temperature isotherms and temperature

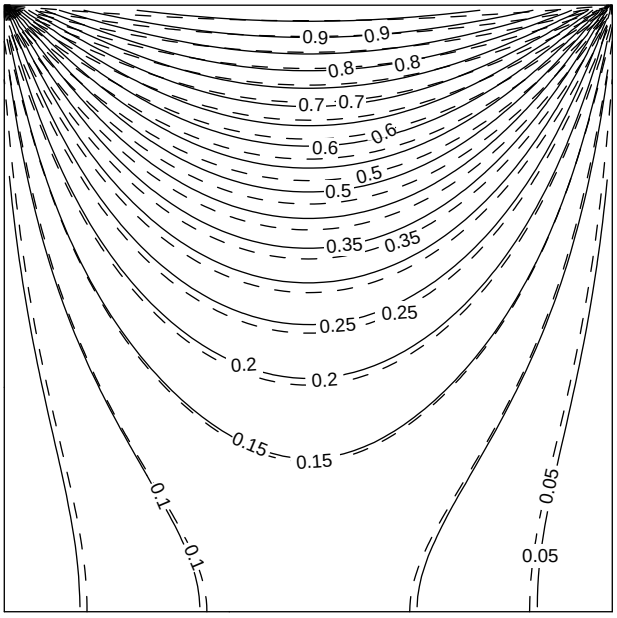

Figure 5. Temperature isotherms for case II (solid line, DPD; dashed line, finite-difference solutions).

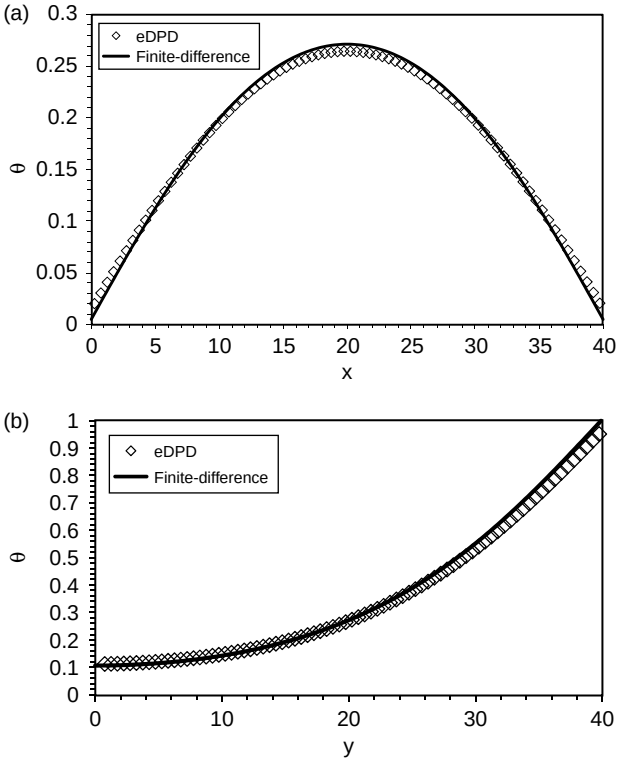

Figure 6. Temperature profiles for case II: (a) section at the mid-slab height (i.e. $y = 20$) and (b) section at the mid-slab width (i.e. $x = 20$).

profiles at the mid-section in the x and y directions, respectively. As revealed from the figures, a good comparison is presented.

4.2 Case II

The geometry and the corresponding boundary condition of this problem are shown in Figure 4(b). The left, right and bottom walls are treated similar to the previous sections. The top wall is exposed to convection heat transfer coefficient h (W/m^2 K).

The heat balance at the top wall surface is written as

$$q''_{\text{conduction}} = q''_{\text{convection}}, \quad -k\frac{\mathrm{d}T}{\mathrm{d}y} = h(T_w - T_{\text{C}}), \qquad (20)$$

where T_{C} is the ambient temperature. Solving for the temperature gradient at the boundary and using Equation (18), the temperature at the top wall is expressed as

$$T_{M,j} = \frac{2T_c(Bi/H) + 4T_{M-1,j} - T_{M-2,j}}{(3 + 2(Bi/H))}, \qquad (21)$$

where Bi is the Biot number given as

$$Bi = \frac{hH}{k},$$

where H is the height of the slab, which is equal to 40. The Biot number plays an essential role in conduction problems where convection effects are involved. It is viewed as the ratio of the convection at the surface to conduction within the solid or the conduction resistance within the solid divided by the convection resistance at the surface [26]. In Equation (21), M, $M-1$ and $M-2$ correspond to the top wall, the first interior cell adjacent to the top wall and the second interior cell adjacent to the top wall, respectively. The value of Bi is varied between 0 (corresponding to perfectly insulated surface) and ∞ (i.e. corresponding to the surface temperature equals the surrounding temperature) to show a wide range of results for the convection-type problems. Figure 7 shows the isotherms using the wide range of Bi. As shown from these simulations, a good comparison between the eDPD solutions and the finite-difference solution is observed. Further comparison is presented in Figure 8 for the case of $Bi = \infty$ showing temperature profiles at the mid-height and width of the slab, and it is concluded from the figures that a good comparison is observed.

4.3 Case III

In the third case, 2D conduction with internal heat generation is investigated. The governing equation describes the heat transfer with internal heat generation, which is given as [24]:

$$\left(\frac{\partial^2 T}{\partial x^2} + \frac{\partial^2 T}{\partial y^2}\right) + \frac{\dot{Q}}{k} = 0, \qquad (22)$$

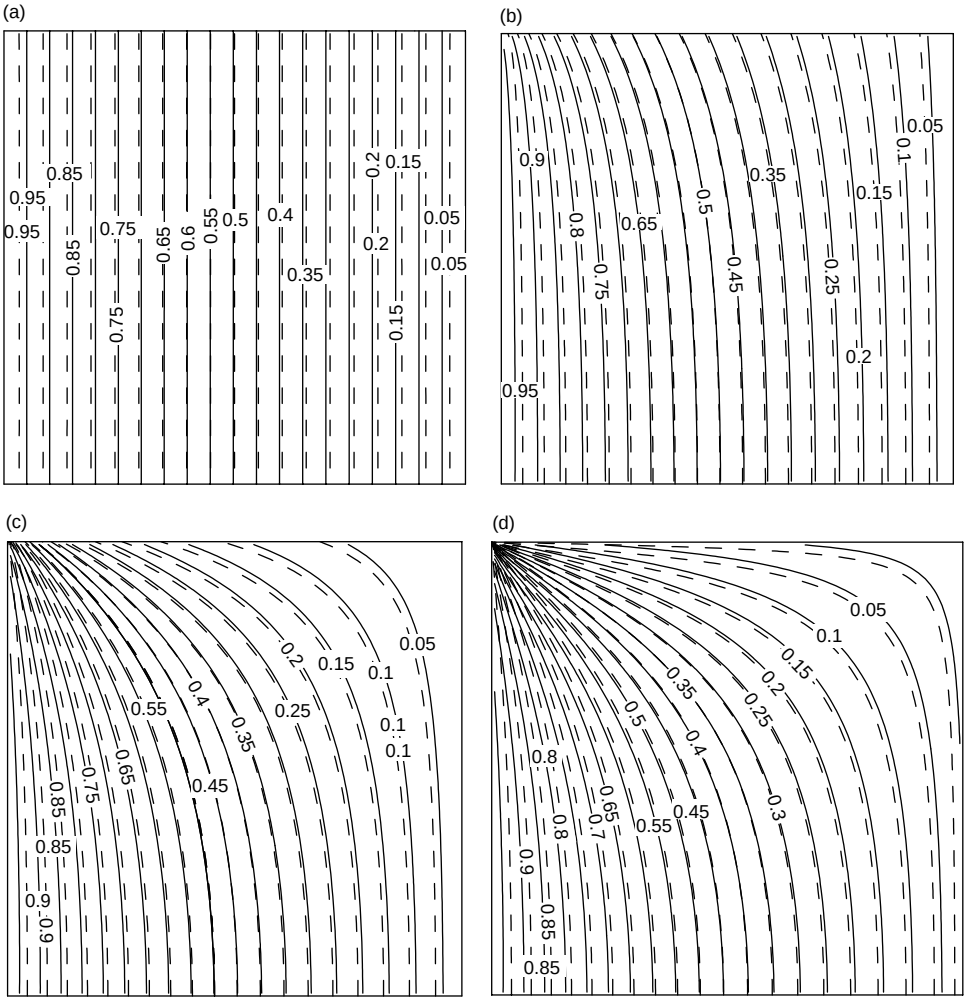

Figure 7. Temperature isotherms for case II (solid line, DPD; dashed line, finite-difference solution): (a) $Bi = 0$, (b) $Bi = 1$, (c) $Bi = 10$ and (d) $Bi = \infty$.

where $\dot{Q}$ is the rate of heat generation per unit volume (W/m^3) and k is the thermal conductivity (W/m K). The following non-dimensional temperature is introduced to compare the DPD with the finite-difference solutions:

$$\theta = \frac{T - T_C}{\dot{Q}H^2/k}. \tag{23}$$

Using Equation (23), Equation (22) can be written as

$$\left(\frac{\partial^2\theta}{\partial x^2} + \frac{\partial^2\theta}{\partial y^2}\right) = -1. \tag{24}$$

The DPD solution is compared to the finite difference, and from this comparison the thermal conductivity and, accordingly, the thermal diffusivity are evaluated. The calculation procedure of thermal diffusivity utilises the non-dimensional analysis by means of the equality of non-dimensional numbers. Using non-dimensional analysis, one can write the following relations:

$$\theta_{DPD} = \theta_{FD}$$

$$\theta_{\max DPD} = \theta_{\max FD}, \tag{25}$$

where FD stands for the finite-difference solution and max is the maximum. The solution of Equation (24) is straightforward and therefore the value of $\theta_{\max FD}$ is known and, accordingly, the value of $\theta_{\max DPD}$ becomes a known quantity using the relation given in Equation (25). Therefore, Equation (23) can be rearranged at maximum temperature as

$$\frac{\dot{Q}}{k} = \left(\frac{T_{\max} - T_C}{H^2}\right)\left(\frac{1}{\theta_{\max DPD}}\right). \tag{26}$$

Consequently, the right term on the right-hand side becomes a known quantity.

The eDPD solution of Equation (22) starts from modifying the energy equation of the eDPD particles to

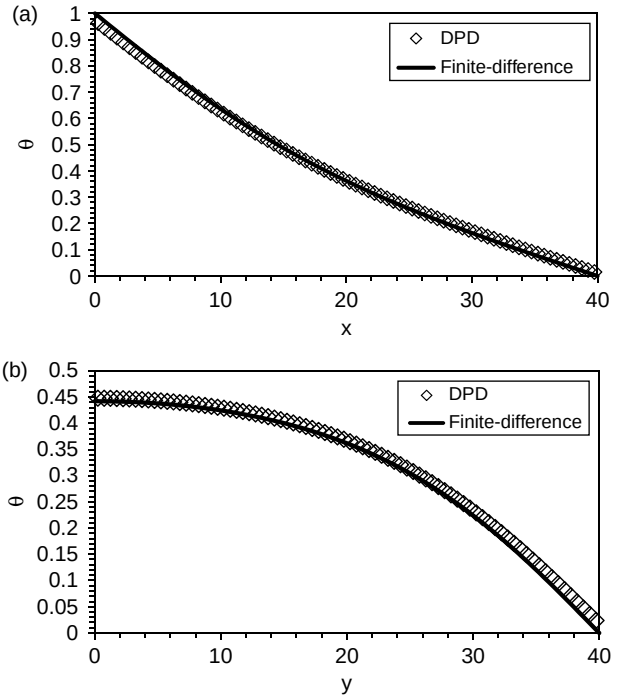

Figure 8. Temperature profiles for case II and $Bi = \infty$. (a) Section at the mid-slab height (i.e. $y = 20$) and (b) section at the mid-slab width (i.e. $x = 20$).

include a heat generation term and, accordingly, the modified equation reads as

$$C_v \frac{\mathrm{d}T_i}{\mathrm{d}t} = \left(q_{ij}^{\mathrm{visc}} + q_{ij}^{\mathrm{cond}} + q_{ij}^{\mathrm{R}}\right) + \dot{Q}(r_c)^2. \qquad (27)$$

In all of the simulations, the r_c is taken as unity. As shown from the problem geometry (Figure 4(c)), all wall boundaries are assigned to the ambient temperature. Therefore, the potential that is driving the heat transfer in the domain is the heat generation term and not the temperature difference between given reservoirs as constantly used by all previous studies in the literature.

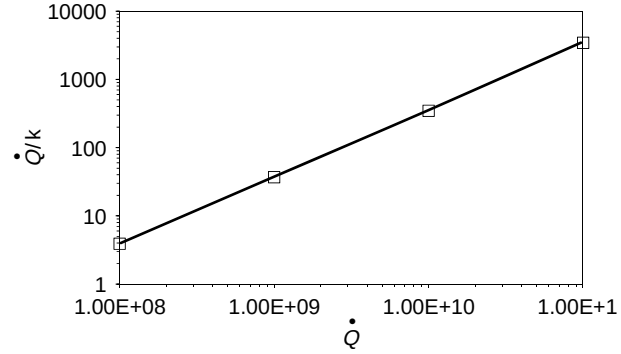

Figure 9. A plot of $\dot{Q}/k$ vs. $\dot{Q}$ for case III to determine the thermal conductivity of the eDPD system.

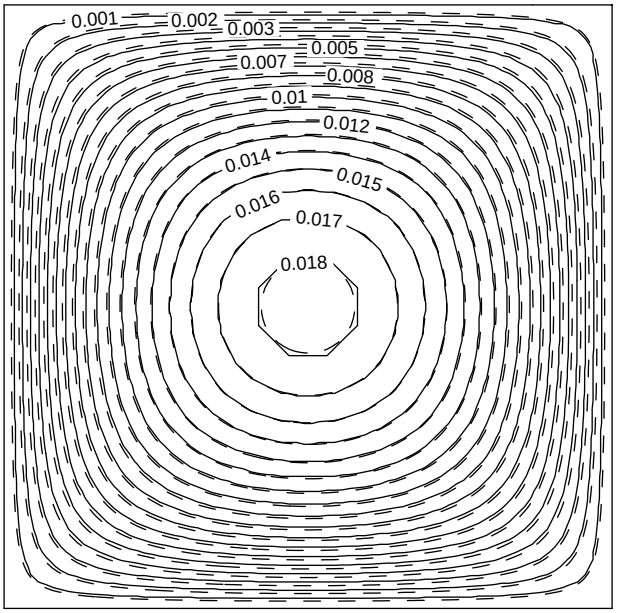

Figure 10. Temperature isotherms for case III (solid line, DPD solution; dashed line, finite-difference).

In the DPD solution, the value of $\dot{Q}$ is varied between 1×10^8 and 1×10^{11}. Therefore, at the steady state, the corresponding quantity $(T - T_C)/H^2$ is known for the

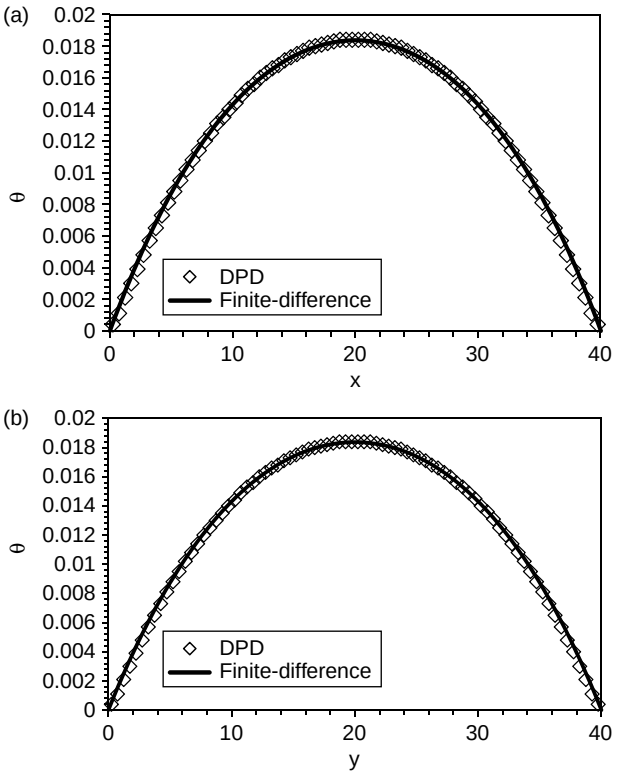

Figure 11. Temperature profiles for case III. (a) section at the mid-slab height (i.e. $y = 20$) and (b) section at the mid-slab width (i.e. $x = 20$).

entire slab domain. Consequently, the right hand side of Equation (26) becomes a known quantity. So, to determine the thermal conductivity of the eDPD system, we plot $\dot{Q}/k$ vs. $\dot{Q}$ and from the slope of the graph one can determine the value of the thermal conductivity. The plot is shown in Figure 9. From the graph, the value of the thermal conductivity is calculated as 3×10^7. Therefore, the thermal diffusivity is determined to be 74.8 (from the relation $D_T = k/(nC_v)$), where n is the number density ($n = 4$) and C_v is the heat capacity of the eDPD system. This procedure was tested for other domain size of (30×30) and (20×20) and gave almost similar results (75 and 75.7, respectively). However, for (10×10), it gave a larger value of 84.1. After the value of the thermal conductivity is obtained, Equation (23) will be used to calculate the non-dimensional temperature of the eDPD domain (since k, $\dot{Q}$ and H are now known quantities). The comparison between the finite-difference solutions of Equation (24) and DPD results is shown in Figures 10 and 11. As shown from the figures, there is almost an exact match between the two approaches.

5. Conclusions

eDPD was applied to investigate steady-state 2D conduction heat transfer using various types of boundary condition. The DPD simulations were compared to analytical and finite-difference solutions. It was found that DPD appropriately predicts the temperature distribution in the conduction regime. The problem of 2D conduction with internal heat generation was studied and the heat generation term was used to measure the thermal conductivity and diffusivity of the eDPD system. The outcome of this study is very helpful for future studies concerned with convection heat transfer.

Acknowledgements

The author would like to thank the Alexander von Humboldt Foundation (AvH) for supporting his research stay at the Leibniz Universität Hannover. Also, the author would like to thank Dr R. Qiao for the useful discussions.

References

[1] P.J. Hoogerbrugge and J.M.V.A. Koelman, *Simulating microscopic hydrodynamic phenomena with dissipative particle dynamics*, Europhys. Lett. 19(3) (1992), pp. 155–160.
[2] R.D. Groot and P.B. Warren, *Dissipative particle dynamics: Bridging the gap between atomic and mesoscopic simulation*, J. Chem. Phys. 107(11) (1997), pp. 4423–4435.
[3] P. Español and P. Warren, *Statistical mechanics of dissipative particle dynamics*, Europhys. Lett. 30(4) (1995), pp. 191–196.
[4] C.A. Marsh, G. Backx, and M. Ernst, *Static and dynamic properties of dissipative particle dynamics*, Phys. Rev. E 55(2) (1997), pp. 1676–1691.
[5] R.D. Groot and K.L. Rabone, *Mesoscopic simulation of cell membrane damage, morphology change and rupture by nonionic surfactants*, Biophys. J. 81 (2001), pp. 725–736.
[6] E.S. Boek, P.V. Coveney, H.N.W. Lekkerkerker, and P.V.D. Schoot, *Simulating the rheology of dense colloidal suspensions using dissipative particle dynamics*, Phys. Rev. E 55(3) (1997), pp. 3124–3133.
[7] X.J. Fan, P.T. Nhan, T.Y. Ng, X.H. Wu, and D. Xu, *Microchannel flow of a macromolecular suspension*, Phys. Fluids 15(1) (2003), pp. 11–21.
[8] J.M.V.A. Koelman and P.J. Hoogerbrugge, *Dynamic simulation of hard-sphere suspensions under steady shear*, Europhys. Lett. 21(3) (1993), pp. 363–368.
[9] M. Liu, P. Meakin, and H. Huang, *Dissipative particle dynamics simulation of multiphase fluid flow in microchannels and microchannel networks*, Phys. Fluids 199 (2007), p. 033302.
[10] C.P. Lowe, *An alternative approach to dissipative particle dynamics*, Europhys. Lett. 47 (1999), p. 145.
[11] A.M. Altenhoff, J.H. Walther, and P. Koumoutsakos, *A stochastic boundary forcing for dissipative particle dynamics*, J. Comp. Phys. 225 (2007), pp. 1125–1136.
[12] J.M. Kim and R.J. Phillips, *Dissipative particle dynamics simulation of flow around spheres and cylinders at finite Reynolds numbers*, Chem. Eng. Sci. 59 (2004), pp. 4155–4168.
[13] P.D. Palma, P. Valentini, and M. Napolitano, *Dissipative particle dynamics simulation of a colloidal micropump*, Phys. Fluids 18 (2006), p. 027103.
[14] S. Chen, N. Phan-Thien, B.C. Khoo, and X.J. Fan, *Flow around spheres by dissipative particle dynamics*, Phys. Fluids 18 (2006), p. 103605.
[15] P. Español, *Dissipative particle dynamics with energy conservation*, Europhys. Lett. 40(6) (1997), pp. 631–636.
[16] J.B. Avalos and A.D. Mackie, *Dissipative particle dynamics with energy conservation*, Europhys. Lett. 40(2) (1997), pp. 141–146.
[17] M. Ripoll, P. Español, and M.H. Ernst, *Dissipative particle dynamics with energy conservation: Heat conduction*, Int. J. Modern Phys. C 9 (1998), pp. 1329–1338.
[18] M. Ripoll and P. Español, *Heat conduction modeling with energy conservation dissipative particle dynamics*, Heat Technol. 18 (2000), pp. 57–61.
[19] R. Qiao and P. He, *Simulation of heat conduction in nanocomposite using energy-conserving dissipative particle dynamics*, Mol. Simul. 33 (2007), pp. 667–683.
[20] P. He and R. Qiao, *Self-consistent fluctuating hydrodynamics simulation of thermal transport in nanoparticle suspensions*, J. Appl. Phys. 103 (2008), p. 094305.
[21] A. Chaudhri and J.R. Lukes, *Multicomponent energy conserving dissipative particle dynamics: A general framework for mesoscopic heat transfer applications*, ASME J. Heat Transfer 131 (2009), p. 033108.
[22] A.D. Mackie, D. Bonet, J.B. Avalos, and V. Navas, *Dissipative particle dynamics with energy conservation: Modeling of heat flow*, Phys. Chem. Chem. Phys. 1 (1999), pp. 2039–2049.
[23] H.S. Carslaw and J.C. Jaeger, *Conduction of Heat in Solids*, 2nd ed., Oxford University Press, New York, 1986.
[24] F.P. Incropera and D.P. Dewitt, *Introduction to Heat Transfer*, 3rd ed., Wiley, New York, 1996.
[25] M.P. Allen and D.J. Tildesley, *Computer Simulations of Liquids*, Clarendon Press, Oxford, 1987.
[26] Y. Çengel and R. Turner, *Fundamentals of Thermal-Fluid Sciences*, 2nd ed., Mc-Graw Hill, New York, 2005.